Spectroscopic Characterization of a Novel Tetranuclear Fe Cluster in an Iron−Sulfur Protein Isolated from *Desulfovibrio desulfuricans*†

Pedro Tavares,‡ Alice S. Pereira,‡ Carsten Krebs,‡ Natarajan Ravi,§ José J. G. Moura,*,|| Isabel Moura,*,|| and Boi Hanh Huynh*,‡

Department of Physics, Rollins Research Building, Emory University, Atlanta, Georgia 30322, Department of Chemistry, Spelman College, Atlanta, Georgia 30314, and Departamento de Química, Faculdade de Ciências e Tecnologia, Universidade Nova de Lisboa, 2825 Monte de Caparica, Portugal

Received September 15, 1997; Revised Manuscript Received December 23, 1997

ABSTRACT: Mössbauer and EPR spectroscopies were used to characterize the Fe clusters in an Fe−S protein isolated from *Desulfovibrio desulfuricans* (ATCC 27774). This protein was previously thought to contain hexanuclear Fe clusters, but a recent X-ray crystallographic measurement on a similar protein isolated from *Desulfovibrio vulgaris* showed that the protein contains two tetranuclear clusters, a cubane-type [4Fe−4S] cluster and a mixed-ligand cluster of novel structure [Lindley et al. (1997) Abstract, Chemistry of Metals in Biological Systems, European Research Conference, Tomar, Portugal]. Three protein samples poised at different redox potentials (as-purified, 40 and 320 mV) were investigated. In all three samples, the [4Fe−4S] cluster was found to be present in the diamagnetic 2+ oxidation state and exhibited typical Mössbauer spectra. The novel-structure cluster was found to be redox active. In the 320-mV and as-purified samples, the cluster is at a redox equilibrium between its fully oxidized and one-electron reduced states. In the 40-mV sample, the cluster is in a two-electron reduced state. Distinct spectral components associated with the four Fe sites of cluster 2 in the three oxidation states were identified. The spectroscopic parameters obtained for the Fe sites reflect different ligand environments, making it possible to assign the spectral components to individual Fe sites. In the fully oxidized state, all four iron ions are high-spin ferric and antiferromagnetically coupled to form a diamagnetic $S = 0$ state. In the one-electron and two-electron reduced states, the reducing electrons were found to localize, consecutively, onto two Fe sites that are rich in oxygen/nitrogen ligands. Based on the X-ray structure and the Mössbauer parameters, attempts could be made to identify the reduced Fe sites. For the two-electron reduced cluster, EPR and Mössbauer data indicate that the cluster is paramagnetic with a nonzero interger spin. For the one-electron reduced cluster, the data suggest a half-integer spin of $^9/_2$. Characteristic fine and hyperfine parameters for all four Fe sites were obtained. Structural implications and the nature of the spin-coupling interactions are discussed.

Iron−sulfur proteins are a class of proteins containing metal cofactors composed of exclusively, or mostly, Fe and S atoms. They are found in all living organisms and play a diverse role in biological functions, including electron transfer, catalysis, iron regulation, and protein structure stabilization (*1*, *2*). The most commonly observed Fe−S cofactors in proteins are the [2Fe−2S], [3Fe−4S], and [4Fe−4S] clusters. Fe−S clusters with Fe nuclearity higher than four and with more elaborate structures are rare in biological systems. However, a complex 8Fe cluster and a mixed-metal 7Fe−Mo cofactor have been found in the nitrogen-fixing enzyme, nitrogenase (*3*). Mixed-metal Ni−Fe clusters have also been found in hydrogenases (*4*) and implicated (by spectroscopic evidence) in CO dehydrogenase (*5*, *6*). Rubredoxin (*2*) and desulforedoxin (*7*), which contain a mononuclear Fe center coordinated by four cysteinyl ligands, are also considered to belong to the class of iron−sulfur proteins.

In 1989, an unusual Fe−S protein was isolated from *Desulfovibrio (D.) vulgaris* (Hildenborough) (*8*). Preliminary characterization of this protein indicated that it contained approximately six Fe atoms per molecule and inorganic sulfur atoms. Upon reduction by dithionite, the protein exhibited an $S = {}^1/_2$ EPR signal distinct from those of the [2Fe−2S] and [4Fe−4S] clusters but resembling that of synthetic compounds with a $[6Fe-6S]^{3+}$ core, termed the prismane core (*9*). Based on these observations, this unusual Fe−S protein was suggested to contain a [6Fe−6S] cluster and the protein was later named the *prismane* protein (*10*). Not long after this initial discovery, an Fe−S protein with similar characteristics was isolated from *D. desulfuricans* (ATCC 27774). A more detailed study, including EPR and Möss-

† This work was supported in part by National Institutes of Health Grant GM 47295 (to B.H.H.) and a grant from PRAXIS XXI (to I. M. and J. J. G. M.). P. T. and A. S. P. are recipients of postdoctoral research fellowships from Programa PRAXIS XXI of Junta Nacional de Investigação Científica e Tecnológica, Portugal. N. R. is supported by a Research Infrastructure in Minority Institutions Award from the National Center for Research Resources with funding from National Institutes of Health Grant RR 11598.

* To whom correspondence should be addressed.
‡ Emory University.
§ Spelman College.
|| Universidade Nova de Lisboa.

S0006-2960(97)02300-3 CCC: $15.00
Published on Web 02/10/1998

bauer characterizations, was performed on the *D. desulfuricans* protein (*11*). On the basis of this study, we concluded that the protein contained two *distinct* multinuclear Fe clusters, termed clusters I and II. Cluster I could be stabilized in several oxidation states, while cluster II could only be stabilized in two oxidation states. In the as-purified protein, cluster I was found to be paramagnetic and exhibited unique Mössbauer and EPR spectra consistent with a spin $S = {}^9/_2$ system. Cluster II was diamagnetic and displayed a Mössbauer quadrupole doublet similar to those of $[4Fe-4S]^{2+}$ clusters. The two clusters showed the same Mössbauer Fe absorption intensity (50:50), suggesting a similar Fe nuclearity for both clusters. At low temperatures (1.5−4.2 K), at least four resolved spectral components were identified to be associated with the paramagnetic Mössbauer spectrum of cluster I. Each spectral component was determined to contribute to 8% of the total Fe absorption. Since approximately 50% of the Fe absorption was associated with cluster I, the observed 8% absorption for each component (corresponding to one Fe site) was then interpreted as evidence supporting a cluster of six Fe atoms. The spectrum of cluster I was then analyzed as a superposition of six spectral components. As only four of the components were resolved, the other two components were assumed to overlap with the spectrum of cluster II. The analysis revealed that the Fe coordination in cluster I was a mixture of N, O, and S ligands. In particular, one of the resolved spectral components exhibited parameters typical of a high-spin ferrous ion with nitrogen and/or oxygen coordination (*11*).

In the dithionite-reduced protein, cluster I was found to undergo a multiple-electron reduction, while cluster II was reduced by one electron. The prismane-like $S = {}^1/_2$ EPR signal observed in the dithionite-reduced protein was attributed to the reduced cluster II, which showed a Mössbauer spectrum similar to that of $[4Fe-4S]^{1+}$ clusters (*11*). However, since both clusters showed the same Fe absorption intensity (i.e., the same nuclearity) and since cluster I was thought to contain six Fe atoms, cluster II was also assigned as a 6Fe cluster, presumably, the prismane-like [6Fe−6S] cluster. In the dithionite-reduced protein, a $S = {}^3/_2$ EPR signal was also observed around $g = 4.7$. The origin of this signal was not determined. The assignment of two distinct 6Fe clusters per molecule (i.e., 12Fe/molecule), however, was noted to be in disagreement with the results of iron determination, which showed five to eight Fe atoms/molecule (*11*). To resolve this apparent discrepancy, we had proposed that the purified samples may contain a mixture of holo- and apo-proteins (*11*).

Extensive physical and biochemical characterizations were also performed on the *D. vulgaris* proteins by Hagen and collaborators (*10*, *12*). Spectroscopic properties very similar to that of the *desulfuricans* protein were observed for the *vulgaris* protein. Moreover, these investigators found, by the application of EPR redox titration, that in addition to the $S = {}^9/_2$ EPR signal of the as-purified protein and the $S = {}^1/_2$ signal of the dithionite-reduced protein, an integer spin EPR signal at $g \sim 16$ was present in an intermediate redox state (*12*). A magnetic circular dichroism study suggested a spin $S = 4$ ground state (*13*).[1] However, based largely on the results of Fe determination and the observed prismane-like $S = {}^1/_2$ signal in the dithionite-reduced protein, these investigators interpreted their data with the premise that only a single Fe cluster was present in the molecule. All the unusual spectroscopic properties mentioned above were therefore attributed to this putative prismane cluster (*10*, *12*, *13*).

The genes encoding both the *D. vulgaris* and *D. desulfuricans* proteins have been cloned, sequenced, and overexpressed in *D. vulgaris* (*14*−*16*). A high degree of homology in the amino acid sequence was observed for the two proteins, and 66% of the residues were found to be identical (*15*). There are nine conserved cysteine residues. Although no sequence homology is found with known sequence motifs that bind Fe−S clusters, four of these residues at the N-terminal region form a sequence motif ($CX_2CX_8CX_5C$) suggestive for binding of an Fe−S cluster (*15*). Similar to the wild-type proteins, the recombinant proteins were found to be able to accommodate multiple redox states, which exhibited optical and EPR spectra similar to those of the wild-type proteins (*14*, *16*). This observation strongly indicates that the Fe clusters in the recombinant and wild-type proteins are similar. Resonance Raman studies of the recombinant proteins (*17*) showed vibrational bands at the 200−430-cm^{-1} region characteristic of Fe−S clusters. Most interestingly, an Fe and O isotope-sensitive band was detected at 801 cm^{-1}, which could be attributed to either an Fe(IV)═O species or a monobridged Fe−O−Fe structure (*17*). This observation, together with our Mössbauer analysis which indicated a mixed N, O, and S ligand environment for cluster I (*11*), suggests an Fe−O−Fe or Fe═O unit as part of the structure for cluster I.

Very recently, the three-dimensional molecular structure of the *D. vulgaris* protein was determined to 1.72-Å resolution (*18*). Most of our earlier conclusions based on the Mössbauer investigation are confirmed by the crystallographic structure, such as, (1) the protein contains two distinct clusters, (2) the two clusters are of the same nuclearity, (3) one cluster has a mixed N, O, S ligand environment, and (4) the other has a regular Fe−S core structure. However, our conclusion on the nuclearity of the clusters is incorrect. They are tetranuclear Fe clusters, not hexanuclear clusters. One cluster is a [4Fe−4S] cluster (cluster II) located at the N-terminal region. The other (cluster I) has a most unusual structure that has never been discovered in any known protein (Figure 1). Two of the Fe atoms (Fe_5 and Fe_6) are bridged by two inorganic sulfide ions, and the other two (Fe_7 and Fe_8) are bridged by a single oxo group, while one Fe atom from each pair (Fe_6 and Fe_8) is linked to each other through a sulfur and an oxo group. The cluster is coordinated to the protein by residues E268, H244, C312, C406, C434, C459, and E494. Most interestingly, ligation of C406 to Fe_8 is through a persulfide group (*18*).

From the crystallographic structure, it is obvious that "prismane protein" is not an appropriate term for describing this protein. A new term is therefore required. Since the protein is brownish in color and since the protein can stabilize the Fe clusters in various redox states, we propose to name this protein *fuscoredoxin*, until the physiological function of this protein is found. To prevent further confusion and to facilitate discussions among different research groups, we

[1] The magnetic circular dichroism study was performed on recombinant *D. vulgaris* proteins.

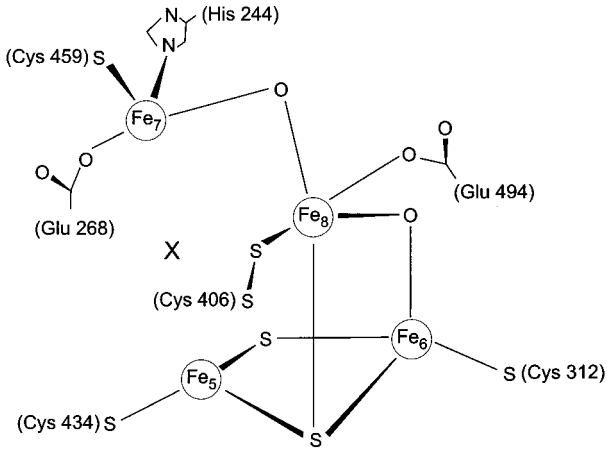

FIGURE 1: Schematic drawing of cluster 2. X represents a proposed possible substrate binding site (adapted from ref 18).

propose to follow the nomenclature used in the crystallographic study (*18*) and use "cluster 1" (formerly cluster II) for the [4Fe−4S] cluster and "cluster 2" (formerly cluster I) for the tetranuclear cluster with novel structure.

The error we made in determining the Fe cluster nuclearity was caused by our assumption that in the as-purified fuscoredoxin, cluster 2 is in a pure $S = {}^9/_2$ state. In retrospect, this assumption was false and unnecessary. In fact, the observation of four resolved, equal intensity (8% of total Fe absorption) spectral components associated with the $S = {}^9/_2$ species in the as-purified protein is consistent with cluster 2 being a tetranuclear Fe cluster. The $4 \times 8 =$ 32% Fe absorption for the four components indicates that only 64% of clusters 2 are in the $S = {}^9/_2$ state (the total Fe absorption for cluster 2 is 50% of the total Fe absorption). The remaining clusters 2 are in a different oxidation state, the spectrum of which is unresolved from that of cluster 1. With such a realization, we have reanalyzed the Mössbauer data of the as-purified *D. desulfuricans* fuscoredoxin. The results of this analysis is presented below. In this paper, we also report a Mössbauer and EPR investigation on two samples prepared at redox potentials different from that of the as-purified protein, one more oxidized and the other further reduced. Cluster 1 was found to be in the $[4Fe-4S]^{2+}$ state in all three samples, while cluster 2 was found to be redox active in the range of redox potentials under studied. Characteristic parameters for cluster 2 in its fully oxidized (4Fe(III)), one-electron reduced (Fe(II), 3Fe(III)) and two-electron reduced (2Fe(II), 2Fe(III)) states are obtained.

MATERIALS AND METHODS.

Sample Preparation. Bacterial growth (in ^{57}Fe-enriched medium) and protein purification were performed as previously described (*11*). The as-purified protein sample was in 100 mM Tris−HCl buffer at pH 7.6. Samples poised at the desired redox states were prepared by using the redox titration method. Protein solution was kept at room temperature in an electrochemical cell that has been described previously (*19*), under positive pressure of argon (prepurified argon, passed through an oxygen trap). Several mediator dyes (methylene blue, indigo tetrasulfonate, 2-hydroxy-1,4-naphthoquinone, anthraquinone, 2-sulfonate, phenosafranine, benzyl viologen, methyl viologen, and *N*,*N*-dimethyl-3-methyl-4,4-bipyridyl) were added to the protein solution to a final concentration of 5 μM each. The redox potentials were measured using a platinum and a saturated calomel standard electrodes (calibrated with quinhydrone at controlled pH) and were quoted relative to the standard hydrogen electrode. The reaction mixture was buffered with 100 mM Tris-HCl at pH 7.6. Reduction or oxidation of the protein was accomplished by additions of aliquots of buffered sodium dithionite, reduced methyl viologen or potassium ferricyanide solutions by using a gas−tight Hamilton syringe. Methyl viologen was reduced by incubation with hydrogen in the presence of trace amounts of *D. desulfuricans* (ATCC 27774) hydrogenase. After equilibration at a desired redox potential, a sample was transferred to an EPR tube or a Mössbauer cuvette which were attached anaerobically to the electrochemical cell. The final protein concentration was 145 μM for the EPR samples and between 600 and 800 μM for the Mössbauer samples. The sample volume was ~200 μL for the EPR samples and 400 μL for the Mössbauer samples. In this paper, we report the results obtained for the as-purified protein as well as for the samples poised at 320 and 40 mV. All chemicals used were of reagent grade or the highest available purity.

Spectroscopic Methods. The weak-field and strong-field Mössbauer spectrometers were operating in a constant-acceleration mode in a transmission geometry and have been described previously (*11*). The zero velocity of the Mössbauer spectra referred to the centroid of the room-temperature spectrum of a metallic iron foil. The EPR spectra were recorded on either a Bruker ER 200D-SRC or a Bruker ESP 300 spectrometer. Both spectrometers are equipped with a dual-mode cavity (Model ER4116DM) and an Oxford Instruments continuous flow cryostat.

RESULTS

EPR Spectra. The EPR data of the as-purified *D. desulfuricans* fuscoredoxin have been reported (*11*). Here, we will briefly summarize those results that are relevant to our analysis of the following Mössbauer data. Basically, the as-purified fuscoredoxin exhibited an unusual EPR signal at the low-field region, consistent with a spin $S = {}^9/_2$ system with a rhombicity $E/D = 0.062$. Temperature dependence of the signal further indicated that the system had a negative zero-field-splitting parameter ($D < 0$). By correlating these information with the observed Mössbauer data, it was concluded that the signal was originating from cluster 2 (*11*). The 320-mV sample shows an EPR spectrum similar to that of the as-purified protein but with a ~40% reduction in signal intensity, suggesting a shift in the equilibrium of cluster 2 toward a higher oxidation state.

Figure 2 shows the 4.2 K EPR spectra of the 40-mV sample recorded with the magnetic component of the microwave perpendicular (spectrum A) and parallel (spectrum B) to the scanning external applied field. Spectrum A can be compared with that of the as-purified sample, which was also recorded with the fields oriented perpendicular to each other. The $S = {}^9/_2$ signal observed in the as-purified protein is absent in the 40-mV sample. Instead, an asymmetric signal with a peak at $g \sim 15$ is observed. In the parallel orientation (spectrum B), the intensity of this signal increases substantially. This behavior is characteristic of an

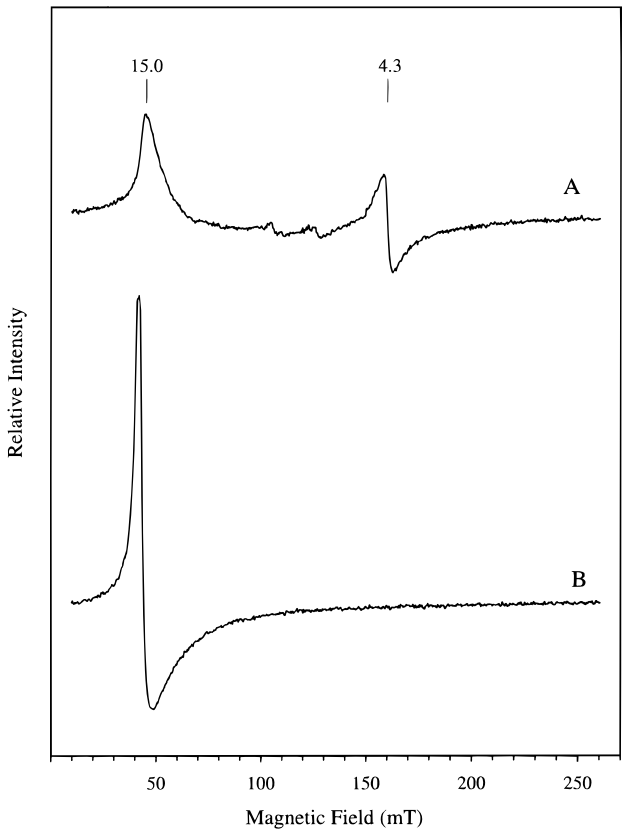

FIGURE 2: EPR spectra of the two-electron reduced fuscoredoxin from *D. desulfuricans* (ATCC 27774). The spectra were recorded with the magnetic component of the microwave aligned perpendicular (A) or parallel (B) to the direction of the external magnetic field. Other experimental conditions are as follows: temperature, 4.2 K; microwave frequency, 9.64 MHz (perpendicular) or 9.37 MHz (parallel); microwave power, 6.2 mW; modulation amplitude, 0.9 mT; receiver gain, 8.0×10^4.

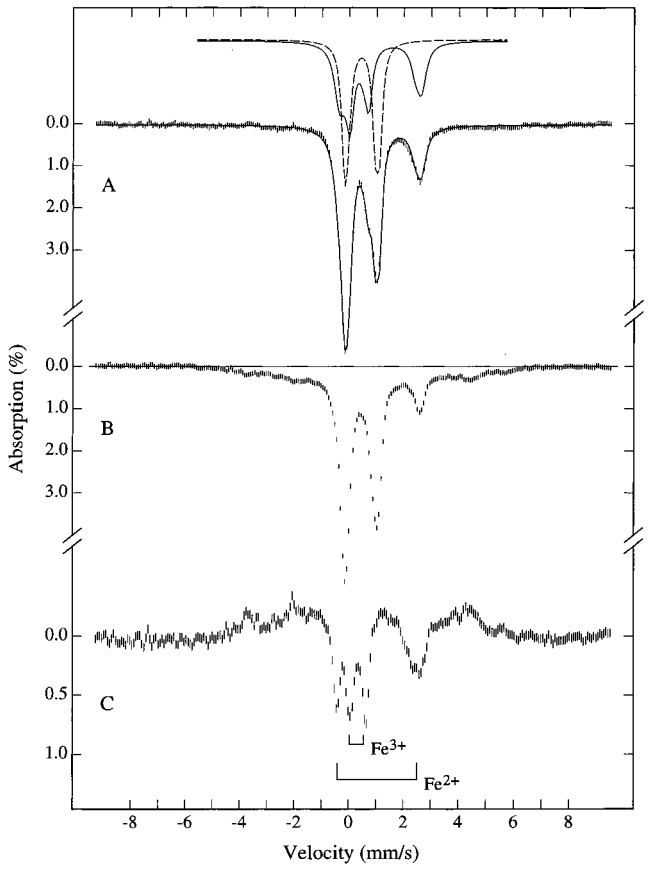

FIGURE 3: Mössbauer spectra of *D. desulfuricans* fuscoredoxin poised at 40 mV. The data were recorded at 4.2 K in the absence of an external field (A) and in the presence of a field of 50 mT (B) applied parallel to the γ-beam. Spectrum C is a difference spectrum between spectra A and B. The solid line plotted over spectrum A is a sum of the theoretical spectra of the oxidized cluster 1 (dashed line shown on top of the data) and the two-electron reduced cluster 2 (solid line shown on top of the data).

integer spin system in which the $\Delta m_S = 0$ transitions, normally forbidden in a perpendicular orientation, become allowed transitions in a parallel configuration (*20*). Similar signals have been observed in the *D. vulgaris* fuscoredoxin (*12*) as well as in the recombinant *D. desulfuricans* protein (*16*). In the *D. vulgaris* protein, the peak is at $g \sim 16$ (*12*). The Mössbauer data, presented below, indicate that this signal is originating from cluster 2 and represents a two-electron reduced state of the cluster. The signal observed in spectrum A at $g = 4.3$ represents a small amount of ferric impurity.

Mössbauer Data. In the following, Mössbauer spectra of the as-purified, 40-, and 320-mV samples are presented. Analysis of these data is made complicated by the fact that the protein contains two multinuclear Fe clusters. In addition, cluster 2 is present in an equilibrium between two oxidation states in the as-purified sample as well as in the 320-mV sample. These complexities result in spectra that are superpositions of overlapping spectral components with various Fe absorption intensities. Consequently, a unique solution cannot be obtained by analysis of any one single spectrum. Instead, the entire set of Mössbauer data of all three samples recorded under different experimental conditions has to be considered as a whole in the analysis. A solution that is consistent with all the available data has been obtained and is presented below. Fortunately, in all three samples, cluster 1 was found to remain in the same $[4Fe-4S]^{2+}$ oxidation state, facilitating the data analysis. This observation is not surprising since the midpoint potential for the $[4Fe-4S]^{2+}/[4Fe-4S]^{1+}$ couple is generally in the −200- to −400-mV region (*2*). Exceptions do exist but are rare.

Fuscoredoxin at 40 mV. Figure 3 shows the 4.2 K Mössbauer spectra of the 40-mV sample recorded in the absence of a magnetic field (spectrum A) and with an external field of 50 mT applied parallel to the γ-beam (spectrum B). In the 50-mT spectrum, two spectral components with comparable Fe absorption intensity can be identified: an intense central quadrupole doublet and a broad magnetic spectrum extending from −6 to +6 mm/s. A similar central quadrupole doublet has also been observed in the spectrum of the as-purified fuscoredoxin recorded under the same experimental conditions (*11*, also, see below). This doublet was found to represent a diamagnetic species and was attributed to cluster 1 in its oxidized form (*11*). Observation of such a doublet in the 40-mV sample with approximately half the Fe absorption indicates that cluster 1 remains in the oxidized form at this potential. In the zero-field spectrum (Figure 3A), only quadrupole doublets are observed, indicating that the broad magnetic component observed in the 50-mT spectrum has collapsed into quadrupole doublets, a property that is unique for integer-spin systems. For an integer-spin system, the degeneracy of the spin multiplet is generally lifted by the ligand field. In the absence of an applied field, this lack of degeneracy results

Table 1: Mössbauer Parameters for Cluster 2 of Fuscoredoxin from *D. desulfuricans* (ATCC 27774)

		fully oxidized		one-electron reduced[b]		two-electron reduced	
iron site	parameters[a]	4.2 K	140 K	4.2 K	140 K	4.2 K	140 K
Fe_5	oxidation state	high-spin Fe^{3+}		high-spin Fe^{3+}		high-spin Fe^{3+}	
	δ (mm/s)	0.27 ± 0.03	0.23 ± 0.03	0.26 ± 0.03	0.24 ± 0.03	0.27 ± 0.03	0.24 ± 0.03
	ΔE_Q (mm/s)	-0.62 ± 0.05	0.58 ± 0.05	-0.60 ± 0.05	0.58 ± 0.05	0.57 ± 0.05	0.56 ± 0.05
	η	3.0 ± 0.5		3.0 ± 0.5			
	$A_{xx}/g_n\beta_n$ (T)			$+8.0 \pm 1.0$			
	$A_{yy}/g_n\beta_n$ (T)			$+8.0 \pm 1.0$			
	$A_{zz}/g_n\beta_n$ (T)			$+7.0 \pm 0.5$			
	Γ (mm/s)	0.4	0.4	0.4	0.40	0.46	0.33
Fe_6	oxidation state	high-spin Fe^{3+}		high-spin Fe^{3+}		high-spin Fe^{3+}	
	δ (mm/s)	0.36 ± 0.03	0.32 ± 0.03	0.35 ± 0.03	0.32 ± 0.03	0.37 ± 0.03	0.32 ± 0.03
	ΔE_Q (mm/s)	-0.72 ± 0.05	0.69 ± 0.05	-0.7 ± 0.05	0.69 ± 0.05	0.68 ± 0.05	0.67 ± 0.05
	η	5.0 ± 1.0		5.0 ± 1.0			
	$A_{xx}/g_n\beta_n$ (T)			-7.8 ± 1.0			
	$A_{yy}/g_n\beta_n$ (T)			-7.8 ± 1.0			
	$A_{zz}/g_n\beta_n$ (T)			-7.8 ± 0.5			
	Γ (mm/s)	0.4	0.4	0.4	0.40	0.27	0.26
Fe_7	oxidation state	high-spin Fe^{3+}		high-spin Fe^{3+}		high-spin Fe^{2+}	
	δ (mm/s)	0.41 ± 0.03	0.35 ± 0.03	0.40 ± 0.03	0.35 ± 0.03	1.04 ± 0.03	1.01 ± 0.03
	ΔE_Q (mm/s)	-0.82 ± 0.05	0.81 ± 0.05	-0.8 ± 0.05	0.81 ± 0.05	2.88 ± 0.05	2.78 ± 0.05
	η	10.0 ± 1.0		10.0 ± 1.0			
	$A_{xx}/g_n\beta_n$ (T)			-11.5 ± 1.5			
	$A_{yy}/g_n\beta_n$ (T)			-9.5 ± 1.0			
	$A_{zz}/g_n\beta_n$ (T)			-9.9 ± 0.5			
	Γ (mm/s)	0.31	0.37	0.4	0.40	0.42, 0.50[c]	0.50, 0.33[c]
Fe_8	oxidation state	high-spin Fe^{3+}		high-spin Fe^{2+}		high-spin Fe^{2+}	
	δ (mm/s)	0.4 ± 0.03	0.34 ± 0.03	1.13 ± 0.03	1.08 ± 0.03	1.15 ± 0.03	1.12 ± 0.03
	ΔE_Q (mm/s)	1.10 ± 0.05	1.2 ± 0.05	3.0 ± 0.05	2.89 ± 0.05	2.98 ± 0.05	2.89 ± 0.05
	η	2.0 ± 0.5		5.0 ± 1.0			
	$A_{xx}/g_n\beta_n$ (T)			-8.0 ± 1.5			
	$A_{yy}/g_n\beta_n$ (T)			-8.0 ± 1.5			
	$A_{zz}/g_n\beta_n$ (T)			-5.3 ± 0.6			
	Γ (mm/s)	0.3	0.31	0.4	0.37	0.47, 0.38[c]	0.36, 0.33[c]

[a] $\eta = (V_{xx} - V_{yy})/V_{zz}$ is the asymmetry parameter, where V_{ii} are the principal components of the electric field gradient at the Fe nucleus, and $g_n\beta_n$ is the magnetic moment of the ^{57}Fe nucleus. [b] Other parameters used in the simulation for the one-electron reduced state are $E/D = 0.062$ and $D = -0.7$ cm^{-1}. [c] The values listed are for the left and right lines of the quadrupole doublet.

in a spin expectation value of zero for each state within the multiplet (*21*). In other words, there is no internal field at the Fe nucleus. Consequently, only quadrupole doublets are observed. The presence of a small external applied field, however, could induce a significant spin expectation value for an integer spin system, which, in turn, would generate an internal field at the Fe nucleus resulting in a magnetic Mössbauer spectrum. As the central quadrupole doublet is attributed to cluster 1, the magnetic component has to be arising from cluster 2. The Mössbauer data are therefore in agreement with the EPR data presented above which show the presence of an integer spin signal at $g \sim 15$. The Mössbauer data further demonstrate that the signal is arising from cluster 2.

Since cluster 1 is diamagnetic, its spectrum is not affected by the application of a small applied field. A difference spectrum between spectra 3A and 3B will cancel the contribution from cluster 1 and reveal the positions of the quadrupole doublets associated with the integer-spin species (i.e., cluster 2). Figure 3C shows such a difference spectrum. Two quadrupole doublets can be identified, one with parameters typical of high-spin Fe^{2+} and the other typical of high-spin Fe^{3+} (marked in Figure 3C). Note that the positions of the ferric quadrupole doublet are different from the peak positions of the central doublet originating from cluster 1 and that the high-energy line of the ferrous doublet is well-resolved from the rest of the spectrum. Consequently, the absorption intensity for the ferrous doublet can be estimated accurately (from spectrum 3A) and is found to be $24\% \pm 3\%$, which corresponds to two Fe atoms. Knowing that cluster 2 contains both ferric and ferrous ions (from the difference spectrum) and that it is a tetranuclear cluster of integer spin, the other two Fe must be ferric. In other words, in the 40-mV sample, cluster 2 is present at a two-electron reduced state.

With the above understanding, it has become possible to analyze the zero-field spectrum (Figure 3A) in detail. Characteristic parameters for the two tetranuclear clusters resulting from this analysis are listed in Tables 1 and 2. A spectral simulation based on this analysis is plotted as a solid curve over the experimental data. Simulations for the individual clusters are also plotted at the top of Figure 3.

As-Purified Fuscoredoxin. Figure 4 shows the Mössbauer spectra of the as-purified fuscoredoxin recorded at 1.5 K with a field of 50 mT applied parallel to the γ-beam (A) and at 4.2 K with a parallel field of 8 T (B). The weak-field spectrum shows clearly the presence of two spectral components: a central quadrupole doublet and a magnetic spectrum extending from -7 to $+8$ mm/s with well-resolved peaks. This spectrum has been reported previously and has been analyzed in detail (*11*). The magnetic component was attributed to cluster 2 and was shown to be arising from a uniaxial system consistent with the ground state of a spin $S = {}^9/_2$ multiplet with $E/D = 0.062$ and $D < 0$ (*11*). For a

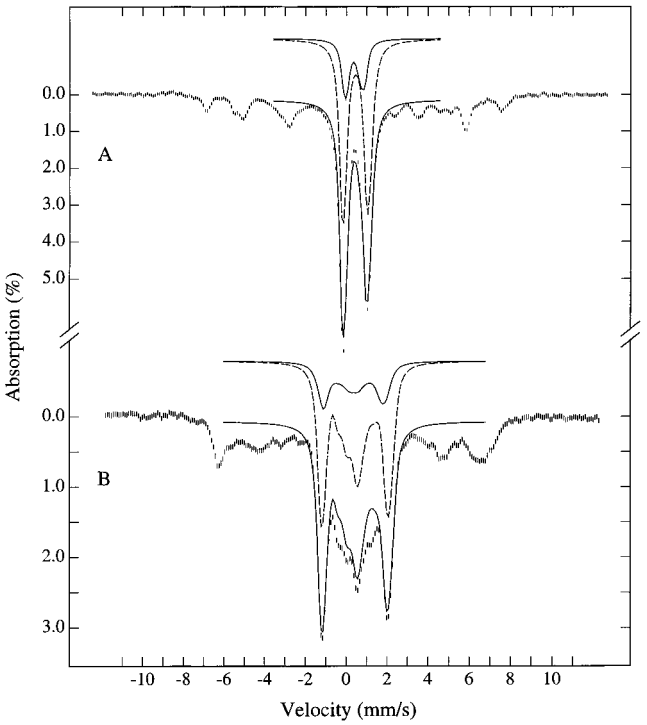

FIGURE 4: Mössbauer spectra of the as-purified *D. desulfuricans* fuscoredoxin. The data were recorded at 1.5 K (A) or 4.2 K (B) with a field of 50 mT (A) or 8 T (B) applied parallel to the γ-beam. The solid lines plotted over the experimental spectra are superpositions of theoretical spectra of the oxidized cluster 1 (dashed lines shown above the data) and fully oxidized cluster 2 (solid lines shown above the data).

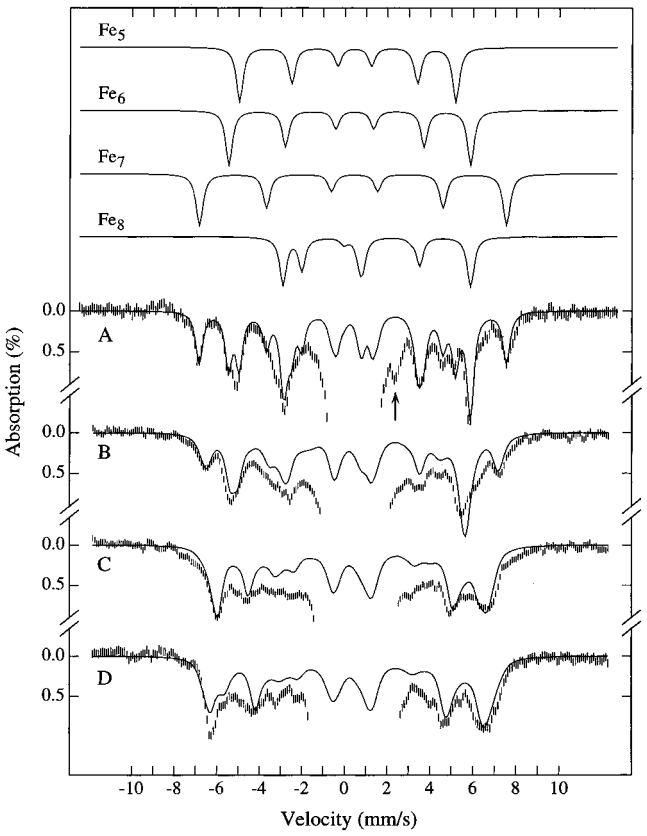

FIGURE 5: Field-dependent Mössbauer spectra of the one-electron reduced cluster 2. The spectra were recorded at 1.5 K (A) or 4.2 K (B−D) with magnetic fields of (A) 50 mT, (B) 3 T, (C) 6 T, and (D) 8 T applied parallel to the γ-beam. The solid lines plotted over the experimental data are theoretical simulations by using the parameters listed in Table 1. Theoretical simulations for the individual iron sites in 50 mT are shown on top of the figure. The arrow in A indicates the position of the high-energy line of the quadrupole doublet of the ferrous impurity.

single Fe site in a uniaxial system, its weak-field Mössbauer spectrum shows a simple six-line pattern with an absorption intensity ratio of 3:2:1:1:2:3. Since the magnetic component shows more than six lines, it was obvious that the spectrum was originating from a multinuclear cluster. In our earlier analysis (*11*), the magnetic spectral component was assumed to be a superposition of six subspectral components, even though only four six-line components are resolved. Due to the high resolution observed for the magnetic component at weak field and the well-defined pattern of the subspectral components, the percent absorption for each subspectral component can be estimated and was found to contribute about 8% of the total Fe absorption. All these above-mentioned observations remain valid except that the number of subspectral components which made up the magnetic spectrum should only be four rather than six, since cluster 2 is a tetranuclear cluster. This is in agreement with the fact that only four resolved six-line subspectral components are observed. Reevaluation of the Mössbauer data of the as-purified fuscoredoxin is therefore required.

Similar to our earlier studies (*11*), we apply a spin-Hamiltonian formulism to analyze the magnetic spectral component. In this analysis, the magnetic component is treated as a superposition of four subspectral components of equal intensity arising from four iron sites. All the iron sites share the same $S = {}^9/_2$ electronic state with $D < 0$ and $E/D = 0.062$ as determined from the EPR data (*11*). The individual Fe sites, however, are found to have different magnetic hyperfine **A** tensors and ΔE_Q and δ values. The difference in the **A** tensors can be explained as a consequence of spin coupling among the Fe atoms, resulting in different spin projections along the system spin of $S = {}^9/_2$, and the difference in ΔE_Q and δ is a reflection on the different ligand environments and oxidation states of each individual Fe site. The results of this analysis are presented in Table 1 and Figure 5. To show the resolution of the magnetic spectral component at weak field and its field-strength dependence in detail, the central portions of the spectra (which are mostly contributions from cluster 1) are not shown in Figure 5. The solid lines plotted over the experimental data are theoretical simulations using the parameters listed in Table 1. With this set of parameters, the field-strength dependence of the magnetic component is properly simulated up to 8 T. Simulations of the four subspectral components at 50 mT are plotted at the top of Figure 5, showing the assignment for the four individual components. This assignment is practically identical to our earlier assignment for the four resolved spectral components. As mentioned in our previous study (*11*), with the highly resolved peaks observed in the magnetic spectrum recorded at 50 mT, this is the only assignment that could explain both the weak- and strong-field spectra. Based on the ΔE_Q and δ values obtained for the individual Fe atoms (see Table 1), this assignment indicates that the magnetic component is originating from a tetranuclear cluster composed of three high-spin ferric and one high-spin ferrous ions, a result that is consistent with the magnetic component representing a half-integer spin (*S*

$= {}^9/_2$) system. This result also suggests that the $S = {}^9/_2$ state of cluster 2 represents the one-electron reduced state of the cluster. The large δ value of 1.13 mm/s determined for the ferrous component suggests N and O ligand environment. In the Discussion section we will argue that this ferrous component is associated with Fe_8 defined in the X-ray structure (*18*, see also Figure 1). The origins of the other three components can also be inferred from the parameters (see Discussion section) and the suggested identities of the Fe sites are labeled in Figure 5 and are listed in Table 1.

A major conclusion resulting from this analysis is that Fe_5 has a positive **A** tensor and that the other sites have negative **A** tensors (Table 1), providing insight into the spin-coupling nature of the one-electron reduced state of this novel cluster (see Discussion section). Due to the significance of this conclusion, a brief explanation is given here to provide confidence on the signs of the **A** tensors determined from our analysis. As mentioned above, the EPR data (*11*) indicate that the electronic ground state for this one-electron reduced cluster 2 is uniaxial. With the highly resolved spectrum recorded in a weak applied field of 50 mT (Figure 5A), the magnitude of the *A* component along the uniaxis (the *z* axis) for each Fe site can be determined accurately from the total splitting of the individual spectrum corresponding to the Fe site (spectra shown above Figure 5A). Once the magnitude of *A* is determined, the sign of *A* can be obtained from the field-strength dependence of the individual spectrum. For a positive *A* value, the total splitting of the spectrum increases with the strength of the applied field, and for a negative *A* value, the splitting decreases with field strength. For the three high-spin ferric sites, the **A** tensors are rather isotropic. Determination of their signs is therefore straightforward. For the ferrous site (Fe_8), the **A** tensor is anisotropic. Determination of its sign is more involved. Nevertheless, with the A_{zz} value determined from the 50-mT spectrum, assumption of a positive **A** tensor results in a simulated 80-T spectrum showing absorption outside of the experimental 80-T spectrum at the positive velocity region. Consequently, only a negative **A** tensor can be assigned to Fe_8.

In the beginning of this section, we mentioned that in order to obtain a unique and self-consistent solution, the whole set of Mössbauer data has to be considered as a whole in the analysis. An example of such a consideration is in the determination of the ΔE_Q and δ values of individual Fe sites. For example, since the $S = {}^9/_2$ state is a one-electron reduced state of cluster 2, the reduced Fe site should also be present in the two-electron reduced state. In other words, the parameters determined for the reduced Fe_8 in the as-purified sample should also be present in the 40-mV sample. Note that in Table 1, an Fe^{2+} site with similar parameters is reported for both the $S = {}^9/_2$ and the two-electron reduced cluster 2. Similarly, the parameters obtained for the two ferric sites in the two-electron reduced state should match two of the three ferric sites in the one-electron reduced cluster 2.[2] Also, the parameters obtained at low temperatures have to be consistent with the parameters obtained from high-temperature spectra after correcting for second-order Doppler shifts (see below).

In the weak-field spectrum (Figure 5A), an absorption peak at 2.25 mm/s is observed (marked by an arrow). In our earlier study (*11*), this peak was mistaken as the outer line of a fifth subspectral component originating from a (currently known) nonexistent fifth Fe site. On the basis of the position of this peak and the fact that its intensity is preparation dependent, we have attributed it to the high-energy line of a ferrous impurity. For the sample shown in Figures 4 and 5, the percent absorption for this ferrous impurity is estimated to be ~2%. It is important to point out that the positions of the high-energy lines of the two ferrous doublets of the two-electron reduced cluster 2 at 2.5 and 2.6 mm/s are distinct from that of the ferrous impurity. The lack of these ferrous lines in the spectrum shown in Figure 4A indicates the absence of the two-electron reduced state of cluster 2 in the as-purified fuscoredoxin.

Since fuscoredoxin contains two tetranuclear clusters, each cluster should contribute approximately 50% of the Fe absorption. The fact that the magnetic spectral component contributes only 32% of the total Fe absorption indicates that cluster 2 is present in an equilibrium between different oxidation states. Since the two-electron reduced state is absent in the as-purified sample, the cluster must be in equilibrium between the fully oxidized all-ferric state and the one-electron reduced $S = {}^9/_2$ state. Based on the above argument, cluster 1 should contribute approximately 50% of the total Fe absorption, while the fully oxidized cluster 2 should contribute ~16%. An all-ferric tetranuclear cluster is expected to have an integer electronic spin and exhibit quadrupole doublets overlapping with those of cluster 1 in the central region of the spectrum shown in Figure 4A. In other words, the intense central quadrupole doublet is composed of spectra originating from both cluster 1 and cluster 2 in their fully oxidized forms. Since these two components are not resolved, albeit different, their characteristic parameters cannot be obtained by a straightforward least-squares fitting of the central doublet without proper constraints. Fortunately, the 320-mV sample contains a significantly higher concentration of fully oxidized cluster 2. By analyzing the spectra of the as-purified sample and the 320-mV samples simultaneously, we were able to deconvolute the central doublet into its two contributing components. The procedure of such an analysis is described in the next paragraph.

Fuscoredoxin at 320 mV. Figure 6 shows the Mössbauer spectra of the 320-mV sample recorded at 4.2 K in a parallel field of 50 mT. Similar to the as-purified fuscoredoxin, the 320-mV sample also exhibits a spectrum consisting of a magnetic spectral component and a central quadrupole doublet. However, the intensity of the magnetic component has reduced significantly in comparison with that of the as-purified protein, indicating a shift in the equilibrium of cluster 2 toward higher oxidation state. By using the most outer peaks at -7 and $+8$ mm/s of the magnetic spectrum, the absorption intensity of the magnetic component can be estimated accurately and was found to be 19% of the total absorption. This is to be compared with the 32% determined

[2] This reasoning obviously can only be true if the reduced electron is localized in one particular Fe site and has little or no effect on the state of the other Fe atoms. Localization of the electron is supported by the Mössbauer data which show well-defined high-spin ferrous components. Evidence to support the lack of effect on other Fe sites is not as strong. However, the agreement between the theoretical simulations and experimental data suggests that it is a reasonable assumption.

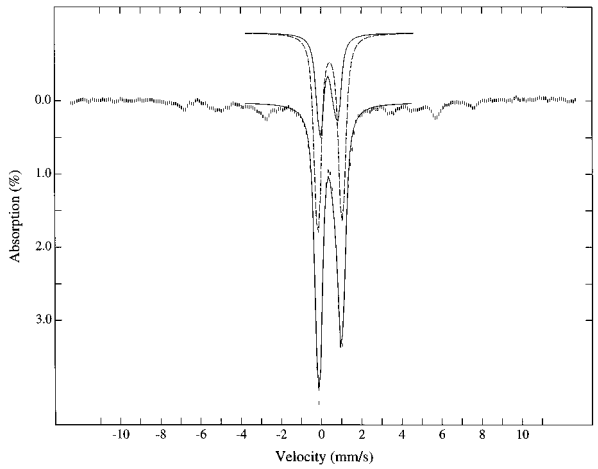

FIGURE 6: Mössbauer spectrum of *D. desulfuricans* fuscoredoxin at 320 mV. The spectrum was recorded at 4.2 K with a magnetic field of 50 mT applied parallel to the γ-beam. The solid line plotted over the central part of the spectrum is a sum of the theoretical spectra of the oxidized cluster 1 (dashed line shown above the data) and the fully oxidized cluster 2 (solid line shown above the data).

for the magnetic component in the as-purified sample. Consequently, in the 320-mV sample, the majority of cluster 2 is in the fully oxidized form and contributes approximately 30% to the total Fe absorption, while the contribution of cluster 1 remains the same (~50% of the total absorption) as in the as-purified sample. This difference in the relative contribution of cluster 1 vs that of oxidized cluster 2 between the 320-mV and the as-purified samples is the key for deconvolution of the central doublet into its two spectral components. The procedure is as follows. The central quadrupole doublet of either sample was prepared from the raw data by the removal of the proper contribution of the magnetic component. For the first iteration of the analysis, a theoretical spectrum of the oxidized cluster 2 was simulated by using parameters obtained for the ferric sites of the one-electron reduced and two-electron reduced cluster 2. By using such a theoretical spectrum, the proper amount of cluster-2 contribution was subtracted from the prepared spectrum of the central quadrupole doublet. The remaining spectrum should therefore represent an approximate spectrum of cluster 1 and was least-squares fitted with two equal intensity quadrupole doublets (to properly represent the shape of the spectrum of oxidized cluster 1, which is presumably a $[4Fe-4S]^{2+}$ cluster, it requires a minimum of two doublets). The parameters obtained for cluster 1 from both samples were compared, and the average values were used to simulate a theoretical spectrum of cluster 1, which was then used to remove the contribution of cluster 1 from the prepared experimental spectrum of the central doublet. The remaining spectrum would then represent an approximation of the spectrum of oxidized cluster 2 and was fitted with four equal-intensity quadrupole doublets with constraints derived from the results obtained for the one-electron reduced and two-electron reduced cluster 2. The parameters obtained were then used for the simulation of a spectrum of cluster 2 for the second iteration. The entire process was then repeated until the parameters obtained from both samples were in agreement within the experimental errors. The results of such an analysis are listed in Tables 1 and 2. Please note that the listed parameters are also in agreement with the corresponding values obtained for the 40-mV samples. Theoretical simulations for the central doublets for the two samples are plotted over the experimental data in Figures 4A and 6. The spectra of the oxidized cluster 1 (dashed line) and fully oxidized cluster 2, normalized with proper absorption intensities, are plotted above the corresponding experimental spectra shown in Figures 4A and 6.

Spectra recorded at strong fields show that both oxidized clusters are diamagnetic. Figure 4B shows the spectrum of the as-purified sample recorded in a parallel field of 8 T. The solid line plotted over the experimental data is a superposition of the simulated spectra of oxidized clusters 1 and 2 by using the parameters obtained above and by assuming diamagnetism for both clusters (i.e., no internal field). The individual simulations for cluster 1 (dashed line) and for the fully oxidized cluster 2 (solid line) are also shown above the experimental spectrum. The plotted spectrum of cluster 1 is normalized to 50% and the spectrum of cluster 2 is normalized to 16% of the total Fe absorption. The observed agreement between experiment and simulation supports the assumption that both oxidized clusters are diamangetic.

Mössbauer Spectra at 140 K. Figure 7 shows the 140 K spectra of the 40-mV (A), as-purified (B), and 320-mV (C) samples. At 140 K, the electronic relaxation is fast in comparison with the ^{57}Fe nuclear precession, resulting in cancellation of the internal field caused by thermal averaging of the fluctuating electronic spins. Consequently, only quadrupole doublets are observed. Consistent with the low-temperature data, which indicate that cluster 1 remains in the same $[4Fe-4S]^{2+}$ state in all three samples, these 140 K spectra also show the presence of a quadrupole doublet (marked by a bracket) attributable to a $[4Fe-4S]^{2+}$ cluster with approximately 50% Fe absorption intensity. Redox potential dependence of cluster 2 is also clearly observable in these spectra. Most notably, an absorption line at ~2.5 mm/s, a position that is typical for the high-energy line of a high-spin ferrous quadrupole doublet, increases in intensity with decreasing redox potential. As the oxidation state of cluster 1 was found to be constant among these three samples, the increase in intensity of the ferrous doublet(s) provides a measure of the extent of reduction of cluster 2. Since this absorption line is well-resolved from the rest of the spectrum, the absorption intensity of the ferrous doublet-(s) in these samples can be estimated accurately and was found to be ~5%, 8%, and 24%, respectively, for the 320-mV, as-purified, and 40-mV samples (the percent absorption for the ferrous impurity found in these samples, ~2%, has been excluded). The 24% ferrous absorption found in the 40-mV sample is in perfect agreement with the low-temperature finding that cluster 2 is at a two-electron reduced state. Most interestingly, the percent ferrous absorptions, 5% and 8%, found for the 320-mV and as-purified samples, respectively, are practically identical to those found for the ferrous component of the magnetic spectrum detected at low temperatures. This observation is consistent with and in support of two major assumptions used throughout our analysis: (1) the paramagnetic $S = {}^9/_2$ state of cluster 2 is a one-electron reduced state, and (2) in the as-purified and 320-mV samples, cluster 2 is in an equilibrium between an all-ferric state and a one-electron reduced state. Also, the line shape of the ferrous high-energy line at ~2.5 mm/s of the 40-mV sample is different and broader in comparison with

Table 2: Mössbauer Parameters for the Oxidized Cluster 1 in *D. desulfuricans* Fuscoredoxin Poised at Different Redox Potentials

		320 mV		as-purified		40 mV	
		4.2 K	140 K	4.2 K	140 K	4.2 K	140 K
doublet 1	δ (mm/s)	0.44 ± 0.03	0.42 ± 0.03	0.45 ± 0.03	0.42 ± 0.03	0.45 ± 0.03	0.42 ± 0.03
	ΔE_Q (mm/s)	1.39 ± 0.05	1.30 ± 0.05	1.34 ± 0.05	1.30 ± 0.05	1.29 ± 0.05	1.28 ± 0.05
	η			0.5 ± 0.2			
	Γ_L, Γ_R (mm/s)	0.29, 0.35	0.26, 0.26	0.35, 0.35	0.27, 0.24	0.27, 0.25	0.39, 0.34
doublet 2	δ (mm/s)	0.44 ± 0.03	0.40 ± 0.03	0.44 ± 0.03	0.39 ± 0.03	0.43 ± 0.03	0.40 ± 0.03
	ΔE_Q (mm/s)	1.06 ± 0.05	1.03 ± 0.05	1.04 ± 0.05	1.03 ± 0.05	1.02 ± 0.05	1.01 ± 0.05
	η			1.0 ± 0.2			
	Γ_L, Γ_R (mm/s)	0.28, 0.30	0.36, 0.35	0.35, 0.35	0.33, 0.33	0.28, 0.26	0.34, 0.36

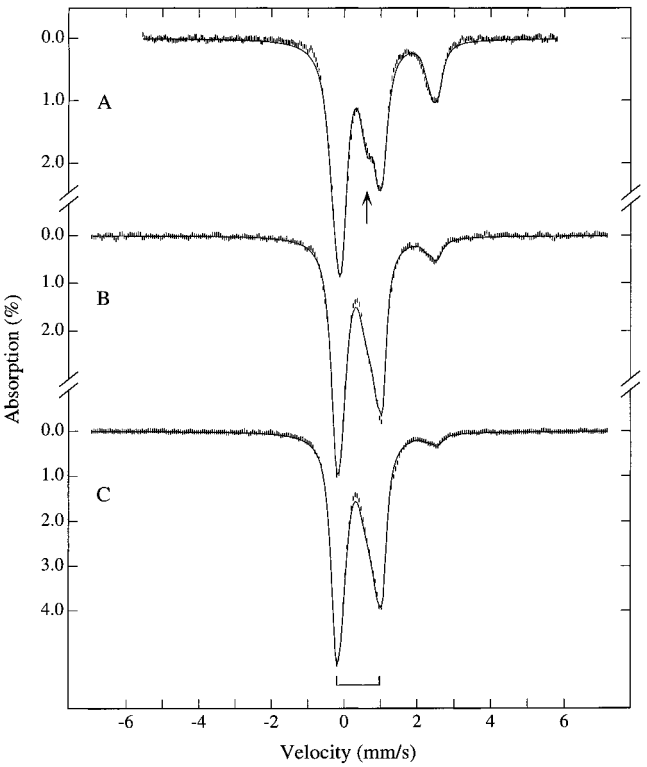

FIGURE 7: Mössbauer spectra of *D. desulfuricans* fuscoredoxin at different redox states: (A) 40 mV, (B) as-purified, and (C) 320 mV. The spectra were recorded at 140 K in the absence of an external magnetic field. The bracket shows the positions of the quadrupole doublet of the oxidized cluster 1, and the arrow indicates the position of the high-energy line of the quadrupole doublet arising from the ferric sites of the two-electron reduced cluster 2. The solid lines plotted over the data are theoretical simulations by using the parameters listed in Tables 1 and 2 (see text).

those of the as-purified and 320-mV samples, indicating that the spectrum of the second reduced Fe atom is different from that of the first reduced Fe atom. Also, with decreasing potential, the intensity of the broad absorption at around 1 mm/s reduces significantly, and a shoulder at ~0.6 mm/s becomes more apparent (indicated by an arrow in Figure 7A). This observation reveals that the ferric sites which convert to the ferrous sites upon reduction must have absorption lines at positions between that of the shoulder and the peak at ~1 mm/s. Interestingly, the position of the shoulder is consistent with those obtained for the ferric sites of the two-electron reduced cluster 2.

The above observations suggest that although the high-temperature spectra consist of mostly unresolved quadrupole doublets, there are sufficient differences among the three spectra to allow for deconvolution of the spectra into their spectral components. A procedure similar to that described above for analysis of the central quadrupole doublet of the low-temperature spectra was applied here. In this analysis, it was assumed that the reduction of cluster 2 was localized at particular Fe sites and that reduction of one Fe did not affect the intrinsic oxidation and spin states of the other Fe atoms in the cluster (see footnote 2). This assumption allows us to simulate the high-temperature spectrum of cluster 2 at different redox potentials with a minimum number of parameters. For example, in the as-purified sample, by correlating the observation that cluster 2 contributes a total of 48% of the total Fe absorption and that the ferrous component contributes 8% of the total Fe absorption, it can be concluded that cluster 2 is at an equilibrium between the fully oxidized and the one-electron reduced state with a population ratio of 1:2, respectively. According to the above assumption, the high-temperature spectrum of cluster 2 in the as-purified sample can be simulated as a superposition of five quadrupole doublets corresponding to the four ferric sites, Fe_5, Fe_6, Fe_7, and Fe_8, and a ferrous site, Fe_8, with percent contributions of 12, 12, 12, 4, and 8%, respectively. Similarly, the spectrum of cluster 2 in the 320-mV sample should consist of the same five doublets, but with percent contributions of 12, 12, 12, 7, and 5%, while the spectrum of cluster 2 in the 40-mV sample is composed of four doublets corresponding to the two ferric sites, Fe_5 and Fe_6, and two ferrous sites, Fe_7 and Fe_8, with an equal contribution of 12% each. With this assumption, we were able to obtain a self-consistent solution and deconvolute the high-temperature spectra into their corresponding spectral components. The results are listed in Tables 1 and 2. The solid lines plotted over the experimental spectra shown in Figure 7 are simulations based on these results. Excellent agreement between the experimental data and the simulations is observed. Again, we would like to emphasize that analyses performed on the high-temperature and low-temperature data are closely correlated. For example, the percent absorption for each component was held constant (i.e., independent of temperature) and the isomer-shift values were expected to reduce by approximately 0.03 mm/s per 100 deg increase in temperature due to the second-order Doppler shifts (*21*).

DISCUSSION

Mössbauer spectroscopy was used to characterize the iron clusters in fuscoredoxin isolated from *D. desulfuricans* (ATCC 27774). Three samples of different oxidation states were examined. One sample contains as-purified protein, and the other two are poised at redox potentials of 40 and 320 mV. Cluster 1 was found to stay at the same oxidation state in all three samples. The Mössbauer parameters obtained for cluster 1 (see Table 2) are typical for a cubane-

type [4Fe−4S] cluster in the 2+ oxidation state (*22*, *23*). Spectra recorded at strong fields indicate further that the cluster is diamagnetic, supporting the 2+ oxidation state assignment. These observations suggest that cluster 1 belongs to the class of ferredoxin-type [4Fe−4S] clusters, which generally has a relatively low midpoint redox potential in the range of −200 to −400 mV for the 2+/1+ couple (*2*). Since cluster 1 is diamagnetic, the previously observed $S = {}^9/_2$ EPR signal in the as-purified protein (*11*) and the currently observed integer-spin EPR signal detected in the 40-mV sample can be attributed to cluster 2. Consistent with the EPR assignment, the Mössbauer data show that cluster 2 is redox active in the potential range studied here and exhibits different Mössbauer spectra in the three samples. Analyses of the Mössbauer data recorded over a wide range of experimental conditions permitted us to determine the redox state of cluster 2 in each sample and to characterize cluster 2 in detail. In the as-purified and 320-mV samples, cluster 2 was found to be at a redox equilibrium between its fully oxidized and one-electron reduced states. In the 40-mV sample, it is reduced to the two-electron reduced state. Four iron sites with different Mössbauer parameters were obtained, reflecting the different ligand environments surrounding the four Fe atoms as revealed in the X-ray crystallographic structure.

In general, it is not possible to determine the ligand environment from Mössbauer parameters. However, with the known structure of cluster 2, it becomes possible to attempt to correlate the different Fe sites observed in the Mössbauer spectra with those defined in the X-ray crystallographic structure. For Fe complexes of the same oxidation and spin state, the Mössbauer isomer shift increases with coordination number and depends on ligand types following the trends that $\delta(\mathrm{O}) > \delta(\mathrm{N}) > \delta(\mathrm{S})$. For example, for high-spin ferrous complexes, the isomer shift of the oxygen-rich Fe(II) sites in methane monooxygenase was reported to be ∼1.30 mm/s (*24*, *25*). For the nitrogen-rich hemerythrin, it was ∼1.1 mm/s (*26*), and for the tetrahedral sulfur-coordinated Fe center in Fe−S proteins, it was ∼0.7 mm/s (*27*, *28*). For the two-electron reduced cluster 2, the two ferrous Fe sites exhibit isomer shifts larger than 1 mm/s and therefore may be assigned to Fe_7 and Fe_8, which are coordinated by mostly N and O ligands. The ferrous site with larger isomer shifts (1.13−1.15 mm/s) is assigned to the five-coordinate Fe_8, while the site with a smaller isomer shift (1.04 mm/s) is assigned to the four-coordinate Fe_7. The ferric sites in the fully oxidized cluster 2 that convert to these two ferrous sites upon reduction can be assigned accordingly by identifying the ferric doublets that are present in the fully oxidized state but are absent in the reduced state. Interestingly, these two ferric sites exhibit isomer shifts (∼0.4 mm/s) that are consistent with those of high-spin ferric ions with mostly N and O ligands. The other two ferric sites are therefore assigned to Fe_5 and Fe_6. The site with the smaller isomer shift, 0.27 mm/s, is assigned to the trisulfur-coordinated Fe_5, and the site with the larger isomer shift, 0.35 mm/s, is assigned to Fe_6, which has an additional oxygen ligand in comparison with Fe_5. According to the above assignment, the first two electrons that reduce cluster 2 are localized at Fe_8 and Fe_7. This appears to be quite reasonable considering the fact that Fe complexes with oxygen ligands generally have midpoint redox potentials higher than that of Fe complexes with sulfur ligands.

The one-electron reduced state of cluster 2 is paramagnetic ($S = {}^9/_2$) and exhibits a well-resolved magnetic spectrum which permits a most detailed characterization of the cluster in this particular oxidation state. In addition to the ΔE_Q and δ values, the component *A* values of the magnetic hyperfine tensor, **A**, were also determined for each iron site. These apparent *A* values reflect the spin-coupling nature of the electronic system. For monomeric Fe centers, the magnetic hyperfine *A* values are negative. The observation of positive *A* values for one of the ferric sites (Fe_5) indicates that the Fe sites are spin-exchange-coupled, resulting in the intrinsic spin of Fe_5 oriented antiparallel to the system spin $S = {}^9/_2$. To gain more detailed information on the spin-coupling and to examine whether the observed *A* values are consistent with the above-proposed assignment, a simple four-spin coupling model for a localized spin system was used. In this model, the intrinsic spins of the ferrous site and the three ferric sites are coupled to form the resultant spin, $S = {}^9/_2$. The four intrinsic spins are represented by the spin vectors $\mathbf{S}_1$, $\mathbf{S}_2$, $\mathbf{S}_3$ and $\mathbf{S}_4$, and the system spin is represented by **S**. The coupling scheme is described as follows:

$$\mathbf{S}_1 + \mathbf{S}_2 = \mathbf{S}_\mathrm{A} \quad \mathbf{S}_\mathrm{A} + \mathbf{S}_3 = \mathbf{S}_\mathrm{B} \quad \mathbf{S}_\mathrm{B} + \mathbf{S}_4 = \mathbf{S} \qquad (1)$$

where $S = {}^9/_2$. With this coupling scheme, the measured apparent *A* value for the *i*th Fe site (A_i) is related to its intrinsic *a* value (a_i) by

$$A_i = C_i\, a_i \qquad (2)$$

where $i = 1$, 2, 3, or 4 and

$$C_1 = \left(\frac{\mathbf{S}_1\cdot\mathbf{S}_\mathrm{A}}{\mathbf{S}_\mathrm{A}^2}\right)\left(\frac{\mathbf{S}_\mathrm{A}\cdot\mathbf{S}_\mathrm{B}}{\mathbf{S}_\mathrm{B}^2}\right)\left(\frac{\mathbf{S}_\mathrm{B}\cdot\mathbf{S}}{\mathbf{S}^2}\right)$$

$$C_2 = \left(\frac{\mathbf{S}_2\cdot\mathbf{S}_\mathrm{A}}{\mathbf{S}_\mathrm{A}^2}\right)\left(\frac{\mathbf{S}_\mathrm{A}\cdot\mathbf{S}_\mathrm{B}}{\mathbf{S}_\mathrm{B}^2}\right)\left(\frac{\mathbf{S}_\mathrm{B}\cdot\mathbf{S}}{\mathbf{S}^2}\right)$$

$$C_3 = \left(\frac{\mathbf{S}_3\cdot\mathbf{S}_\mathrm{B}}{\mathbf{S}_\mathrm{B}^2}\right)\left(\frac{\mathbf{S}_\mathrm{B}\cdot\mathbf{S}}{\mathbf{S}^2}\right)$$

$$C_4 = \left(\frac{\mathbf{S}_4\cdot\mathbf{S}}{\mathbf{S}^2}\right) \qquad (3)$$

The value of S_i can take on either 2 or ${}^5/_2$ provided that for each possible set of $\{S_i\}$, there are three spins equal to ${}^5/_2$ and one spin equal to 2. This coupling scheme yields a total of 60 possible orientations of the 4 spins to form an $S = {}^9/_2$ state. The spin-projection factors, C_i, for each orientation were calculated according to eq 3. Out of these 60 states, there are 13 states in which the spin of a single ferric site is aligned antiparallel to the system spin. The spin orientations of these 13 states and the corresponding spin projection factors are listed in Table 3.

For high-spin ferric ions, the intrinsic **a** tensor is generally rather isotropic and has a value between −17 T (for tetrahedral sulfur-coordinated Fe sites) (*27*, *28*) to −22 T (for oxygen-rich Fe sites) (*29*). By using the average value (7.7 T) of the 3 components of the **A** tensor obtained for the antiparallel ferric site (Fe_5) and the corresponding spin-projection factors listed in Table 3, the intrinsic *a* value for

Table 3: List of Spin-Projection Factors of the 13 $S = {}^9/_2$ States Which Have the Spin of One Single Ferric Site Aligned Antiparallel to the System Spin

	S_1	S_2	S_3	S_4	S_A	S_B	C_1	C_2	C_3	C_4
1[a]	2	$^5/_2$	$^5/_2$	$^5/_2$	$^9/_2$	7	32/77	40/77	40/77	−5/11
2	2	$^5/_2$	$^5/_2$	$^5/_2$	$^9/_2$	6	6728/18 711	8410/18 711	754/2079	−17/99
3	2	$^5/_2$	$^5/_2$	$^5/_2$	$^9/_2$	3	784/2673	980/2673	−28/297	43/99
4[a]	2	$^5/_2$	$^5/_2$	$^5/_2$	$^9/_2$	2	88/243	110/243	−10/27	5/9
5	2	$^5/_2$	$^5/_2$	$^5/_2$	$^7/_2$	6	754/2673	1073/2673	145/297	−17/99
6	2	$^5/_2$	$^5/_2$	$^5/_2$	$^7/_2$	2	338/1701	481/1701	−1/27	5/9
7	2	$^5/_2$	$^5/_2$	$^5/_2$	$^1/_2$	2	8/81	−14/81	14/27	5/9
8[a]	$^5/_2$	$^5/_2$	2	$^5/_2$	5	7	40/77	40/77	32/77	−5/11
9	$^5/_2$	$^5/_2$	2	$^5/_2$	5	6	29/63	29/63	58/231	−17/99
10	$^5/_2$	$^5/_2$	2	$^5/_2$	4	6	116/297	116/297	116/297	−17/99
11	$^5/_2$	$^5/_2$	$^5/_2$	2	5	$^7/_2$	851/2079	851/2079	−23/189	10/33
12	$^5/_2$	$^5/_2$	$^5/_2$	2	5	$^5/_2$	10/21	10/21	−25/63	4/9
13	$^5/_2$	$^5/_2$	$^5/_2$	2	4	$^5/_2$	20/63	20/63	−5/63	4/9

[a] Possible solutions for the one-electron reduced state of cluster 2.

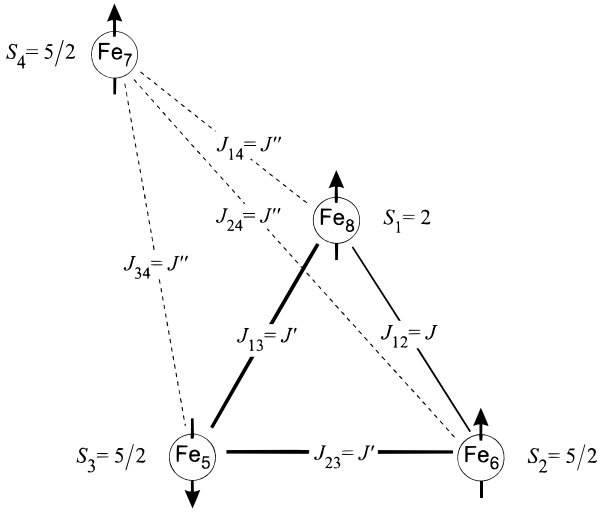

FIGURE 8: Schematic drawing of the spin-orientation and spin-coupling scheme for state 4 listed in Table 3, a possible solution for the one-electron reduced state of cluster 2.

the antiparallel Fe site can be estimated for each of the 13 states by using eq 2. Only states 1, 4, and 8 yield acceptable a values of ~ -20 T. Other states yield much larger a values and are therefore unacceptable. States 1, 4, and 8 also yield reasonable intrinsic a values for the other three sites. To illustrate this point, state 4 is used as an example. For state 4, the two ferric sites with their spins "parallel" to the system spin have different spin-projection factors (see Table 3). According to the magnitudes of the spin-projection factors, the two ferric spins S_2 and S_4 were assigned to the Fe sites Fe_6 and Fe_7, respectively (see Figure 8). This assignment results in reasonable intrinsic a values for the two ferric sites: -17 T for Fe_6 and -19 T for Fe_7. For state 4, the spin S_1 is equal to 2, and therefore, it can only be assigned to Fe_8. By using the spin-projection factor 88/243 for S_1 and the apparent A values determined for Fe_8, the intrinsic **a** tensor for Fe_8 can be estimated. The results are -22, -22, and -15 T for the three principle components of **a**. Due to the large orbital and spin-dipolar contributions, the **a** tensor for high-spin ferrous ion is anisotropic and the values of its components vary over wide ranges. It is therefore interesting to note that the component a values determined for Fe_8 compare relatively well with those (-25, -24, and -11 T) found for the ferrous ion in protocatechuate 3,4-dioxygenase (*30*), an iron site with N and O ligands.

The above analysis indicates that the magnetic hyperfine coupling constants observed for the Fe sites of cluster 2 reveal a spin orientation that can be described reasonably well by state 4. That is, the spins of Fe_8 ($S_1 = 2$) and Fe_6 ($S_2 = {}^5/_2$) are parallel and coupled to form an intermediate spin S_A of $^9/_2$. This intermediate spin is antiferromagnetically coupled to the spin of Fe_5 ($S_3 = {}^5/_2$) to form another intermediate spin, $S_B = 2$, which is then ferromagnetically coupled to the spin of Fe_7 ($S_4 = {}^5/_2$) to form the final spin, $S = {}^9/_2$ (see Figure 8). Basically, all three states 1, 4, and 8 describe similar spin orientation for the four Fe sites. That is, the spin of Fe_5 is antiparallel to the spins of Fe_6, Fe_7, and Fe_8, which are oriented parallel with each other. It is interesting to note that such a spin orientation could also be used to explain the $S = 4$ spin state for the two-electron reduced cluster 2 as suggested by the MCD study (*13*). According to the Mössbauer results presented above, the second reducing electron is localized at Fe_7 and the intrinsic state of Fe_7 in the two-electron reduced cluster 2 is high-spin ferrous. By using the same coupling scheme describing state 4, a ferromagnetic coupling between the high-spin ferrous Fe_7 with the intermediate spin $S_B = 2$ would result in a final spin $S = 4$.

Although state 1, 4, or 8 describes the observed hyperfine coupling constants reasonably well and therefore provides an insight into the spin orientation, it is important to point out that the coupling scheme used above may be too simplistic. A general spin Hamiltonian describing the interactions between four exchange-coupled spins can be written as

$$H = -2\sum_{i<j}^{4} J_{ij}\mathbf{S}_i\cdot\mathbf{S}_j \qquad (4)$$

In formulating the simple coupling scheme presented above, we have assumed that the intermediate spins S_A and S_B are good quantum numbers. In other words, we have assumed the following simpler Hamiltonian for the exchange interactions:

$$H = -2J\mathbf{S}_1\cdot\mathbf{S}_2 - 2J'(\mathbf{S}_1 + \mathbf{S}_2)\cdot\mathbf{S}_3 - 2J''(\mathbf{S}_1 + \mathbf{S}_2 + \mathbf{S}_3)\cdot\mathbf{S}_4 \qquad (5)$$

where $J = J_{12}$, $J' = J_{13} = J_{23}$, and $J'' = J_{14} = J_{24} = J_{34}$. Based on the structure of cluster 2, the above assumptions for the exchange coupling constants cannot be strictly correct.

For example, the exchange coupling constants J_{14}, J_{24}, and J_{34} may not be exactly equal. However, they could be similar. Also, state 1, 4, or 8 may serve as a good approximation for the ground state of the one-electron reduced cluster 2, even though the state is a quantum admixed state of eigen states of the Hamiltonian defined in eq 5.

To find the limits of the exchange coupling interactions within which a state with the spin orientation depicted in Figure 8 is a ground state, a search in the energy space as a function of the exchange coupling constants was performed. The details of this search are the subject of a future report (Krebs et al., Unpublished Results). Interesting results that can be understood intuitively are discussed here. It was found that the spin orientation of Fe_5, Fe_6, and Fe_8 (shown in Figure 8) can be realized with antiferromagnetic coupling between the Fe sites provided that the couplings between Fe_5 and the other two sites are stronger than that between Fe_6 and Fe_8. Based on the structure of cluster 2, antiferromagnetic coupling between these three Fe sites appears to be a reasonable assumption. The spin orientation of Fe_7 (shown in Figure 8) can be obtained by assuming either that (1) the coupling between Fe_7 and Fe_8 is ferromagnetic or (2) Fe_7 is antiferromagnetically coupled to Fe_8 and Fe_5 with the coupling between Fe_7 and Fe_5 being the stronger interaction (the coupling between Fe_7 and Fe_6 is assumed to be weak). Ferromagnetic coupling between Fe_7 and Fe_8 is not quite likely since oxygen bridged spin-localized mixed-valent Fe(II,III) systems with an Fe−O−Fe angle in the range of 113−180° are generally antiferromagnetically coupled (*31*−*35*). To the best of our knowledge, there exists only one ferromagnetically coupled localized Fe(II,III) model compound with a known structure in which the Fe sites are double bridged by two phenoxo groups with an Fe−O−Fe angle of ∼96° (*36*, *37*). Bridge angles close to 90° were suggested to promote ferromagnetic coupling due to the orthogonality of the interacting magnetic orbitals of the Fe ions and the bridging atoms (*37*). Although detailed structural coordination data are not yet available to us, the resonance Raman data of an 801-cm^{-1} asymmetric stretching mode (*17*) suggests an Fe−O−Fe angle of ∼140° (*38*) for cluster 2. The effects of electron transfer between the metal ions have also been suggested to enhance ferromagnetic coupling (*39*, *40*). As the valences of Fe_7 and Fe_8 are localized at 140 K on the Mössbauer time scale, ferromagnetic coupling due to electron transfer may not be significant. The latter possibility also appears to be difficult to rationalize with the available X-ray structure of cluster 2, which shows a possible substrate binding site between Fe_7 and Fe_5, suggesting a weak coupling between the two Fe sites. There remains, however, the possibility that the X-ray structure may represent a structure of the cluster in an oxidation state different from the one-electron reduced state. In this respect, it is interesting to note that for the fully oxidized cluster 2, the state is diamagnetic ($S = 0$). Such a state can be realized with an antiferromangnetic coupling between Fe_7 and Fe_8 as expected with the X-ray structure. Upon one-electron reduction (to Fe_8), a spin flip at the Fe_7 site would form the observed $S = {}^9/_2$ state, which may reflect a conformational change involving Fe_7, Fe_5, and Fe_8.

The property that Fe cofactors in proteins can exist in different oxidation states has long been understood as an essential factor for the function of many Fe-containing proteins. For example, the high-valent Fe(IV) state is important for the function of heme-containing oxygenases (*41*). More recently, it has been realized that in addition to the feasibility of attaining different oxidation states, structural flexibility of certain Fe cofactors also plays a pivotal role in determining enzyme reactivities. For example, the carboxylate-bridged dinuclear Fe cluster in methane monooxygenase has been shown to undergo carboxylate shifts between its oxidized and fully reduced states (*42*, *43*). Spectroscopic and kinetic data further suggest that substantial structural rearrangement is taking place during the enzyme catalytic cycle (*44*). Also, the structure of the 8Fe P cluster in nitrogenase was recently shown to be redox sensitive, and this observed redox-mediated structural change was suggested to be involved in coupling of electron and proton transfers (*45*). In this respect, it is interesting to note that cluster 2 of fuscoredoxin appears to possess both structural flexibility and redox activity. The X-ray crystallographic structure of cluster 2 shows that it consists of a flexible arm, the Fe_7−O−Fe_8 unit, built upon a relatively stable base structure, the bis(μ-S) Fe_5−Fe_6 unit. The spectroscopic study reported here indicates that cluster 2 is redox active and can be stabilized in three different oxidation states. Interestingly, the reducing electrons were found to localize at particular Fe sites. Based on the structure of cluster 2, this localization of the electrons appears to be by design. A previous redox titration study (*11*) further suggested that in addition to the three oxidation states described in this paper, there are two more states attainable at lower redox potentials. Preliminary analysis of protein samples poised at potentials below −100 mV reveals that the persulfide ligand to Fe_8 may be involved in the redox behavior of the cluster. These intriguing properties of cluster 2 all point to a possibly interesting function. Currently, biochemical and molecular biological experiments are planned in order to reveal the physiological function of fuscoredoxin.

REFERENCES

1. Flint, D. H., and Allen, R. M. (1996) *Chem. Rev. 96*, 2315−2334.
2. Johnson, M. K. (1994) *Encyclopedia of Inorganic Chemistry* (King, R. B., Ed.) Vol. 4, pp 1896−1915, John Wiley and Sons, Chichester, U. K.
3. Howard, J. B., and Rees, D. C. (1996) *Chem. Rev. 96*, 2965−2982.
4. Volbeda, A., Charon, M.-H., Piras, C., Hatchikian, E. C., Frey, M., and Fontecilla-Camps, J. C. (1995) *Nature 373*, 580−587.
5. Ragsdale, S. W., and Kumar, M. (1996) *Chem. Rev. 96*, 2515−2539.
6. Xia, J., Hu, Z., Popescu, C. V., Lindahl, P. A., and Münck, E. (1997) *J. Am. Chem. Soc. 119*, 8301−8312.
7. Moura, I., Huynh, B. H., Hausinger, R. P., LeGall, J., Xavier, A. V., and Münck, E. (1980) *J. Biol. Chem. 255*, 2493−2498.
8. Hagen, W. R., Pierik, A. J., and Veeger, C. (1989) *J. Chem. Soc., Faraday Trans. 1 85*, 4083−4090.
9. Kanatzidis, M. G., Salifoglou, A., and Coucouvanis, D. (1985) *J. Am. Chem. Soc. 107*, 3358−3360.
10. Pierik, A. J., Wolbert, R. B. G., Mutsaers, P. H. A., Hagen, W. R., and Veeger, C. (1992) *Eur. J. Biochem. 206*, 697−704.
11. Moura, I., Tavares, P., Moura, J. J. G., Ravi, N., Huynh, B. H., Liu, M.-Y., and LeGall, J. (1992) *J. Biol. Chem. 267*, 4489−4496.

12. Pierik, A. J., Hagen, W. R., Dunham, W. R., and Sands, R. H. (1992) *Eur. J. Biochem. 206*, 705−719.
13. Marritt, S. J., Farrar, J. A., Breton, J. L. J., Hagen, W. R., and Thomson, A. J. (1995) *Eur. J. Biochem. 232*, 501−505.
14. Stokkermans, J. P. W. G., Houba, P. H. J., Pierik, A. J., Hagen, W. R., van Dongen, W. M. A. M., and Veeger, C. (1992) *Eur. J. Biochem. 210*, 983−988.
15. Stokkermans, J. P. W. G., van den Berg, W. A. M., van Dongen, W. M. A. M., and Veeger, C. (1992) *Biochim. Biophys. Acta 1132*, 83−87.
16. Van den Berg, W. A. M., Stevens, A. A. M., Verhagen, M. F. J. M., van Dongen, W. M. A. M., and Hagen, W. R. (1994) *Biochim. Biophys. Acta 1206*, 240−246.
17. De Vocht, M. L., Kooter, I. M., Bulsink, Y. B. M., Hagen, W. R., and Johnson, M. K. (1996) *J. Am. Chem. Soc. 118*, 2766−2767.
18. Lindley, P., Hadden, J., Card, G., McAlpine, A., Bailey, S., Zaitsev, V., Duke, E., Arendsen, A., Bulsink, Y., Hagen, W. R. (1997) Abstract, Chemistry of Metals in Biological Systems, European Research Conference, Tomar, Portugal.
19. Gupta, N., Bonomi, F., Kurtz, D. M., Jr., Ravi, N., Wang, D. L., and Huynh, B. H. (1995) *Biochemistry 34*, 3310−3318.
20. Hendrich, M. P., and Debrunner, P. G. (1989) *Biophys. J. 56*, 489−506.
21. Lang, G. (1970) *Quart. Rev. Biophys. 3*, 1−60.
22. Middleton, P., Dickson, D. P. E., Johnson, C. E., and Rush, J. D. (1980) *Eur. J. Biochem. 104*, 289−296.
23. Middleton, P., Dickson, D. P. E., Johnson, C. E., and Rush, J. D. (1978) *Eur. J. Biochem. 88*, 135−141.
24. Fox, B. G., Hendrich, M. P., Surerus, K. K., Andersson, K. K., Froland, W. A., Lipscomb, J. D., and Münck, E. (1993) *J. Am. Chem. Soc. 115*, 3688−3701.
25. DeWitt, J. G., Bentsen, J. G., Rosenzweig, A. C., Hedman, B., Green, J., Pilkington, S., Papaefthymiou, G. C., Dalton, H., Hodgson, K. O., and Lippard, S. J. (1991) *J. Am. Chem. Soc. 113*, 9219−9235.
26. Clark, P. E., and Webb, J. (1981) *Biochemistry 20*, 4628−4632.
27. Huynh, B. H., and Kent, T. A. (1984) *Adv. Inorg. Biochem. 6*, 163−178.
28. Trautwein, A. X., Bill, E., Bominaar, E. L., and Winkler, H. (1991) *Struct. Bond. 78*, 1−95.
29. Kretchmar, S. A., Teixeira, M., Huynh, B. H., and Raymond, K. N. (1988) *Biol. Metals 1*, 26−32.
30. Zimmermann, R., Huynh, B. H., Münck, E., and Lipscomb, J. D. (1978) *J. Chem. Phys. 69*, 5463−5467.
31. Müller, M., Bill, E., Weyhermüller, T., and Wieghardt, K. (1997) *J. Chem. Soc., Chem. Commun.* 705−706.
32. Neves, A., de Brito, M. A., Vencato, I., Drago, V., Griesar, K., and Haase, W. (1996) *Inorg. Chem. 35*, 2360−2368.
33. Bossek, U., Hummel, H., Weyhermüller, T., Bill, E., and Wieghardt, K. (1995) *Angew. Chem., Int. Ed. Engl. 34*, 2642−2645.
34. Bernard, E., Moneta, W., Laugier, J., Chardon-Noblat, S., Deronzier, A., Tuchagues, J.-P., and Latour, J.-M. (1994) *Angew. Chem., Int. Ed. Engl. 33*, 887−889.
35. Borovik, A. S., Papaefthymiou, V., Taylor, L. F., Anderson, O. P., and Que, L., Jr. (1989) *J. Am. Chem. Soc. 111*, 6183−6195.
36. Surerus, K. K., Münck, E., Snyder, B. S., and Holm, R. H. (1989) *J. Am. Chem. Soc. 111*, 5501−5502.
37. Snyder, B. S., Patterson, G. S., Abrahamson, A. J., and Holm, R. H. (1989) *J. Am. Chem. Soc. 111*, 5214−5223.
38. Sander-Loehr, J., Wheeler, W. D., Shiemke, A. K., Averill, B. A., Loehr, T. M. (1989) *J. Am. Chem. Soc. 111*, 8084−8093.
39. Blondin, G., and Girerd, J.-J. (1990) *Chem. Rev. 90*, 1359−1376.
40. Girerd, J.-J. (1983) *J. Chem. Phys. 79*, 1766−1775.
41. Sono, M., Roach, M. P., Coulter, E. D., and Dawson, J. H. (1996) *Chem. Rev. 96*, 2841−2887.
42. Rosenzweig, A. C., Frederick, C. A., Lippard, S. J., and Nordlund, P. (1993) *Nature 366*, 537−543.
43. Rosenzweig, A. C., Nordlund, P., Takahara, P. M., Frederick, C. A., and Lippard, S. J. (1995) *Chem. Biol. 2*, 409−418.
44. Edmondson, D. E., and Huynh, B. H. (1996) *Inorg. Chim. Acta 252*, 399−404.
45. Peters, J. W., Stowell, M. H. B., Soltis, S. M., Finnegan, M. G., Johnson, M. K., and Rees, D. C. (1997) *Biochemistry 36*, 1181−1187.

BI9723008